P2X7 PET Radioligand ^{18}F-PTTP for Differentiation of Lung Tumor from Inflammation

Zhequan Fu*[1], Qingyu Lin*[1,2], Bingxin Hu[1], Yingying Zhang[1], Weijia Chen[1], Jing Zhu[1], Yanzhao Zhao[1], Hak Soo Choi[3], Hongcheng Shi[1,2], and Dengfeng Cheng[1,2]

[1]Department of Nuclear Medicine, Zhongshan Hospital, Fudan University, Shanghai, China; [2]Shanghai Institute of Medical Imaging, Shanghai, China; and [3]Department of Radiology, Gordon Center for Medical Imaging, Massachusetts General Hospital and Harvard Medical School, Boston, Massachusetts

Site-specific imaging agents play a key role in tumor targeting, but only a few agents are currently available for inflammation targeting. Since the P2X7 receptor (P2X7R) is a promising molecular target for inflammation, we evaluated the potential value of the ^{18}F-labeled tracer ^{18}F-PTTP (5-{[2-Chloro-3-(trifluoromethyl)phenyl]carbonyl}-1-pyrimidin-2-yl-4,5,6,7-tetrahydro-1H-[1,2,3]triazolo[4,5-c]pyridin) for targeting P2X7Rs and thus differentiating inflammation from tumors. **Methods:** The radioligand ^{18}F-PTTP was achieved by a 1-step ^{18}F-trifluoromethylation reaction. The binding affinity of the ligand for P2X7R and its stability were evaluated in vitro. Blood pharmacokinetics tests and biodistribution studies were performed in vivo. Dynamic ^{18}F-PTTP small-animal PET/CT imaging was performed for 60 min on A549 tumor–bearing mice and inflammation-model mice for targeting differentiation. **Results:** ^{18}F-PTTP was afforded with decay-corrected radiochemical yields of 2.5%–7.0%, specific activity of 296–370 MBq/μmol, and radiochemical purity over 95%. ^{18}F-PTTP showed excellent stability in 0.9% NaCl and 0.1% bovine serum albumin, good affinity to RAW264.7 cells, and rapid blood clearance in mice. In inflammation-model mice, uptake of ^{18}F-PTTP peaked at 5 min after injection and kept at an imageable level till 30 min, whereas no significant radioactivity uptake was found in tumor grafts till 1 h after injection. The specificity of ^{18}F-PTTP was verified by blocking studies and histologic analysis. **Conclusion:** The current study provides compelling data that ^{18}F-PTTP is a novel radioligand targeting P2X7R and has potential to screen new drugs, quantify peripheral inflammation, and distinguish inflammation from certain solid tumors.

Key Words: purinergic receptors; P2X7 receptors; inflammation marker; lung tumor

J Nucl Med 2019; 60:930–936
DOI: 10.2967/jnumed.118.222547

Inflammation is a common pathologic process accompanying many diseases, such as cardiovascular disease (*1*), neurodegenerative disorders (*2*), type 2 diabetes mellitus (*3*), and cancers (*4*). A large number of tumor-specific imaging agents have been developed to identify tumors, but few have been designed to target inflammation. There is therefore a need to develop inflammation-specific imaging agents to accurately diagnose and explore the pathogenesis.

Macrophages, as well as other cells of monocyte lineage, are major inflammatory cell types involved in inflammatory responses, immune regulation, tissue repair, and remodeling (*5*). Macrophage-targeted PET radiotracers are a reasonable approach to localize and assess inflammatory tissues (*6*). Until recently, the translocator protein has been the most studied macrophage-targeted biomarker for imaging inflammation tissues using PET (*7*). However, translocator protein polymorphism causes differences in binding affinity of PET radioligands, which makes analysis and interpretation of the translocator protein PET image difficult (*8*). With the further understanding of the structure and function of the P2X7 receptor (P2X7R), researchers have suggested that P2X7R could be a valuable alternative marker for macrophages and neuroinflammation (*9,10*).

P2X7R is expressed mainly in inflammatory and immune-related myeloid cells, especially macrophages and microglia. It is regarded as silent under normal physiologic conditions but functionally upregulated when there is an imbalance in adenosine triphosphate concentration during some pathologic processes (*9*). Activation of P2X7R mediates NLRP3 inflammasome activation, cytokine and chemokine release, T-lymphocyte survival and differentiation, transcription factor activation, and cell death (*11*). P2X7R is a potent stimulant of inflammation and immunity and a promoter of cancer cell growth (*12*). This makes it an appealing target for antiinflammatory and possibly anticancer therapy (*13*).

Several radiolabeled P2X7 ligands have been developed and evaluated. Neither ^{11}C-A740003 (*14*) nor ^{18}F-EFB (*15*) showed appreciable brain uptake; however, ^{3}H-A740003 succeeded in recognizing the site of inflammation in human postmortem brain sections, as well as rodent brain sections when examined by in vitro autoradiography (*16*). ^{11}C-GSK1482160 (*17*) showed great promise due to its strong P2X7 selectivity, efficient radiosynthesis, and blood–brain barrier permeability. Its preclinical evaluation is still in progress. ^{11}C-JNJ54173717 (*18*) and ^{11}C-SMW139 (*19*) were evaluated in the human P2X7R–overexpressing rat model. Both tracers entered the rat brain and showed excellent uptake in the human P2X7R–overexpressing striatum compared with the contralateral striatum. In addition, ^{11}C-JNJ54173717 showed high initial brain uptake in nonhuman primates, which, in all likelihood, will enable ^{11}C-JNJ54173717 to proceed to clinical evaluation (*18*). However, based on the finding that P2X7 upregulation is present in active multiple sclerosis lesions (*16*), ^{11}C-SMW139 is

Received Oct. 29, 2018; revision accepted Dec. 10, 2018.
For correspondence or reprints contact either of the following:
Dengfeng Cheng, Department of Nuclear Medicine, Zhongshan Hospital, 180 Fenglin Rd., Shanghai, China.
E-mail: cheng.dengfeng@zs-hospital.sh.cn
Hongcheng Shi, Department of Nuclear Medicine, Zhongshan Hospital, 180 Fenglin Rd., Shanghai, China.
E-mail: shi.hongcheng@zs-hospital.sh.cn
*Contributed equally to this work.
Published online Jan. 17, 2019.

currently being explored for use in patients diagnosed with multiple sclerosis.

Because ^{11}C-labeled imaging agents are limited, we selected a potent P2X7 antagonist, PTTP (5-{[2-Chloro-3-(trifluoromethyl) phenyl]carbonyl}-1-pyrimidin-2-yl-4,5,6,7-tetrahydro-1H-[1,2,3] triazolo[4,5-c]pyridin), for ^{18}F-labeled inflammation imaging. PTTP has good physicochemical properties, excellent pharmacokinetic characteristics, and strong affinity with hP2X7 and mP2X7, which together make it ideal for an inflammation imaging probe. We designed ^{18}F-PTTP as a new P2X7R-targeted ligand and PET probe. We outline the synthesis and the radiochemical, physical, and biologic characterization of ^{18}F-PTTP and explore its potential for PET imaging of inflammatory tissues and differential imaging of tumors.

MATERIALS AND METHODS

Cell Culture and Protein Extraction

RAW264.7 mouse macrophage cells and A549 human non–small cell lung cancer cells were cultured in Dulbecco modified Eagle medium, and H358, H292, SPC-A1, H460, and H1975 non–small cell lung cancer cells were cultured in RPMI-1640 medium. Both media were supplemented with 10% fetal bovine serum and a 100 IU/mL concentration of penicillin–streptomycin. All cell lines were kept at 37° C in a humidified atmosphere containing 5% CO_2. For measurement of probe uptake in vitro, all cell lines were seeded in 6-well plates with 3×10^5 cells/mL. Cells were grown to 80% confluency and then washed twice with ice-cold phosphate-buffered saline and lysed using radioimmunoprecipitation assay lysis buffer plus 1 mM phenylmethylsulfonyl fluoride (Beyotime Biotechnology). The lysates were collected by scraping from the plates and were centrifuged at 10,000*g* at 4°C for 5 min. The protein concentration in the supernatant was determined by micro–bicinchoninic acid protein assay (Beyotime Biotechnology). Protein samples (10 μg) were diluted into the sample buffer (Beyotime Biotechnology) and then boiled for 5 min and frozen at −80°C.

Immunocytochemistry

Cells were fixed in 4% paraformaldehyde in phosphate-buffered saline for 20 min at room temperature. After washing 3 times with phosphate-buffered saline, cells were first blocked with 1% bovine serum albumin in phosphate-buffered saline for 30 min and then incubated with rabbit antimurine P2X7R antibody (1:100) and rat anti-mCD68 antibody (1:100) overnight at 4°C. After washing 3 times with phosphate-buffered saline, cells were incubated with Alexa Fluor 488–conjugated goat antirabbit (1:400, GB25303; Servicebio) and cyanine dye 3–conjugated goat antirat (1:300, GB21301; Servicebio) for 1 h at room temperature. After 3 triple-washings with phosphate-buffered saline, cell nuclei were stained by 4′,6-diamidino-2-phenylindole for 5 min and images were captured on an Olympus fluorescence microscope (IX73).

Chemistry and Radiochemistry

We designed the synthesis route of the radiolabel precursor pre-PTTP as indicated in Figure 1. Compound 2 was synthesized from 4-chloro-3-nitropyridine and 2-aminopyrimidine, the nitro group having been reduced to amino to give compound 3. Compound 3 was reacted with tert-butyl nitrite to give compound 4, which was hydrogenated to give the critical compound 5. In addition, 2-chloro-3-iodo-benzoic acid was obtained from 3-amino-2-chlorobenzoic acid through iodination of the amino group (b2). It was further transformed to 2-chloro-3-iodobenzoyl chloride by thionyl chloride. Lastly, pre-PTTP was obtained by addition of 2-chloro-3-iodobenzoyl chloride to the amide group of compound 5. In the synthesis, the compounds obtained at each step were followed by proton nuclear magnetic resonance (400 MHz; Bruker) and liquid chromatography mass spectroscopy (LCMS-2020; Shimadzu). Synthesis of ^{18}F-PTTP via the precursor pre-PTTP was performed in a multifunction reaction module (StynthraRNplus; Stynthra) as indicated in the last step of Figure 1. ^{18}F-KF, together with cryptating agent K_{222} in MeCN, was added to a V-vial containing CuI (57 μmol, 11 mg) and a magnetic stirrer bar. The solvent was evaporated under N_2 at 100°C (2 min). The evaporation process was repeated 3 times, and each time 1 mL of dry acetonitrile was added. The vial was removed from heat, and a solution of methyl chlorodifluoroacetate (57 μmol, 6 μL), 1,2-bis(dimethylamino)ethane (57 μmol, 9 μL), and pre-PTTP precursor (6 mg, 13 μmol) in dimethylformamide (300 μL) was added via syringe. The sealed vial was heated at 150°C for 20 min to give the desired ^{18}F-PTTP tracer probe. After the mixture was cooled, the reaction was quenched by addition of water (100 μL), and ^{18}F-PTTP was isolated by reversed-phase high-performance liquid chromatography (HPLC) (1260 Infinity [Agilent]; the mobile phase was 3.5/6.5 MeCN/H_2O with 0.1% trifluoroacetic acid) combined with solid-phase extraction using a C-18 Sep-Pak cartridge.

In Vitro Stability, Pharmacokinetics, and Biodistribution of ^{18}F-PTTP

The in vitro stability in 0.9% NaCl and 0.1% bovine serum albumin was evaluated at 1, 2, 4, and 6 h. Eight-week-old female BALB/c nude mice were injected via the caudal vein with ^{18}F-PTTP at a dose of 0.74 MBq/mouse. For pharmacokinetics studies, blood from the tail vein was collected at serial time points (n = 5/time point). In biodistribution experiments, mice (n = 5/time point) were anesthetized and sacrificed at 5, 10, 15, 30, 60, and 90 min after injection. Blood was obtained by cardiac puncture. The following organs were removed for analysis: thyroid, heart, lung, liver, spleen, kidneys, stomach, intestines (small and large), bones, skeletal muscles, and brain. All samples were weighed, counted via a γ-counter, and decay-corrected to the time of injection. Uptake was presented as percentage injected dose per gram of tissue.

Cell Line Receptor Expression Validation

To validate the P2X7R expression in RAW264.7 mouse macrophage cells, P2X7R and CD68 double-immunocytochemistry labeling was performed. To observe the P2X7R expression difference among RAW264.7 mouse macrophage cells and non–small cell lung cancer cells, H358, H292, SPC-A1, H460, and A549 human non-small cell lung cancer cells were selected for Western blot experiments. Heat-denatured proteins (20 μg) were loaded on 10% sodium dodecyl sulfate polyacrylamide gels for electrophoresis and then transferred onto methanol-activated poly(vinylidene fluoride) membranes (Immobilon-P) for blotting. Membranes were first blocked at room temperature for 1 h with blocking solution (5% skimmed milk in Tris-buffered solution plus Tween-20) and then incubated overnight at 4°C with a rabbit anti-P2X7R antibody (1:200, APR-008; Alomone) and rabbit antiactin (1:1,000, 4970; Cell Signaling Technology) in blocking solution. After three 10-min washings in Tris-buffered solution plus Tween-20 detergent/buffer, membranes were incubated for 1 h at room temperature with a horseradish peroxidase–conjugated antirabbit secondary antibody at 1:1,000 dilution in blocking solution. Detection utilized an enhanced chemiluminescence substrate (ECL, Immobilon; Millipore) using a Western blotting luminol reagent according to the manufacturer's instructions. Bands were quantified by scanning densitometry (Thermal Imaging System FTI-500; Pharmacia Biotech).

Radioligand Binding and Saturation Assays

RAW264.7 mouse macrophage cells were seeded in 24-well plates at a density of 2×10^5 per well and incubated with ^{18}F-PTTP (37 kBq/0.5 mL per well) at 37°C for 15, 30, 60, and 120 min. Cell suspensions were collected individually and measured in a γ-counter. Cell uptake

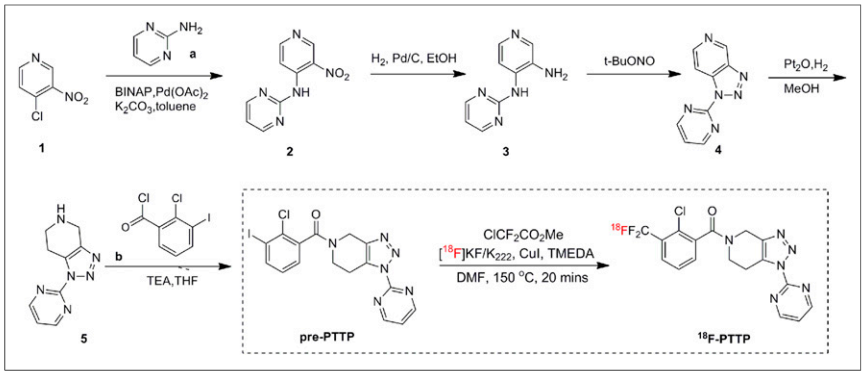

FIGURE 1. Synthetic routes for pre-PTTP and radiosynthesis scheme for ^{18}F-PTTP.

was expressed as a percentage of the decay-corrected, total input radioactivity. For saturation studies, cold ^{19}F-PTTP (100 μM) was added to the RAW264.7 cells. After incubation, the RAW264.7 cell uptake assay was repeated as described above. The cell uptake and saturation measurements were replicated 3 times in triplicate wells. Data are expressed as the percentage added dose after the decay correction.

Animal Models

BALB/c nude mice (female; 6–8 week old; weight, 17–20 g each) were purchased from Shanghai Lingchang Biotechnology and divided into inflammation and solid tumor–bearing groups. The inflammation group was injected intramuscularly with turpentine oil (30 μL) in the left thigh. The solid tumor group consisted of mice subcutaneously injected with A549 cells (4×10^6 in Matrigel, 100 μL) in the right thigh. All mice were housed in a pathogen-free environment under a 12-h light/dark cycle with free access to food and water. Animal care and experimental procedures were approved by the Animals Ethics Committee of Zhongshan Hospital, Fudan University.

Small-Animal PET/CT Imaging

Three tumor-group animals and 3 inflammation-group animals were selected for PET imaging. Before injection of radionuclide tracer (either ^{18}F-FDG or ^{18}F-PTTP), the mice were kept fasting for 4 h. For PET imaging, approximately 11.1 MBq of ^{18}F-FDG or 3.7 MBq of ^{18}F-PTTP were injected in each animal via the tail vein. The mice were anesthetized with isoflurane gas, and PET images were acquired using a whole-body emission protocol on a small-animal PET scanner 0.5 h after ^{18}F-FDG was injected. The ^{18}F-FDG PET scan was performed 1 d before the ^{18}F-PTTP dynamic PET/CT scan (Inveon; Siemens). Blocking studies were performed to evaluate the P2X7R specificity of ^{18}F-PTTP in vivo. Mice in the inflammation group ($n = 3$) were intravenously injected with 1 mg of cold ^{19}F-PTTP 10 min before the radiolabeled ^{18}F-PTTP was administered. Dynamic PET/CT scans were acquired immediately after ^{18}F-PTTP injection and were continued for 0.5 h. Images were reconstructed using a 3-dimensional ordered-subsets expectation-maximization algorithm. CT data were acquired in standard-resolution mode. Three-dimensional regions of interest were manually drawn around tumors on the basis of coregistered CT scans acquired immediately after PET imaging. Mean SUVs were calculated within the region of interest.

Histologic Analysis

At the completion of each imaging session, excised tumors and inflamed tissues of the thigh were fixed in formalin, dehydrated, and embedded in paraffin. Five-micrometer sections of each tissue were stained with hematoxylin and eosin. Double immunofluorescence labeling was performed using a rabbit primary antibody for the murine P2X7R (1:100-fold dilution) and rat anti-mCD68 (1:50-fold dilution). To visualize these primary antibodies, we used Alexa Fluor 488–conjugated goat antirabbit (1:400) and cyanine dye 3–conjugated goat antirat secondary antibodies (1:300). The images were acquired using a fluorescence microscope (Eclipse C1; Nikon).

Statistics

The cell binding kinetics data were analyzed using a nonlinear fit of an association algorithm, whereas binding saturation kinetics was analyzed using a 1-site saturation model, both of which are available in Prism software (version 6.01; GraphPad Software). Statistical analysis of immunocytochemistry staining and P2X7R Western blot analyses were performed using a 1-way ANOVA by SPSS, version 23.0. Tissue biodistribution data were analyzed using a 2-way ANOVA package available in Prism (version 6.02; GraphPad Software). Statistical analysis of image data was performed using the Student t test for comparisons between 2 groups. In all cases, data are presented as mean ± SD, and the ratio of target to normal muscle (T/N) is calculated, where statistical significance was taken at a P value of less than 0.05.

RESULTS

Chemistry and Radiochemistry

The chemical purity of the precursor pre-PTTP was determined to be more than 95% by reversed-phase HPLC using absorbance measurements at 220 and 254 nm. The results of pre-PTTP proton nuclear magnetic resonance were as follows: ($CDCl_3$, 400 MHz) δ 8.89 (d, J = 4.8 Hz, 1H), 8.86 (d, J = 4.8 Hz, 1H), 7.97–7.93 (m, 1H), 7.43–7.38 (m, 1H), 7.33–7.26 (m, 1H), 7.09–7.02 (m, 1H), 5.18–5.03 (m, 1H), 4.60–4.47 (m, 1H), 4.25–4.07 (m, 1H), 3.63–3.53 (m, 1H), 3.44–3.42 (m, 1H), 3.39–3.17 (m, 1H). MS (electrospray ionization): 467.0 ($[M+H]^+$, 100%). The proton nuclear magnetic resonance results for PTTP synthesized according to reference 19 were as follows: ($CDCl_3$, 400 MHz) δ 8.87 (d, J = 4.8 Hz, 1H), 8.83 (d, J = 4.8 Hz, 1H), 7.78–7.73 (m, 1H), 7.51–7.36 (m, 3H), 5.17–5.01 (m, 1H), 4.58–4.43 (m, 1H), 4.32–3.99 (m, 1H), 3.62–3.40 (m, 2H), 3.37–3.17 (m, 1H). The radiochemical yield for the synthesis of ^{18}F-PTTP was 2.5%–7% after decay correction to the end of bombardment based on ^{18}F-HF. The overall synthesis time was about 1.5 h from the end of bombardment. The specific activity of ^{18}F-PTTP was 296–370 MBq/μmol at the end of synthesis as determined by the spike method using analytic HPLC. The radiochemical purity of ^{18}F-PTTP was over 95% as determined by radio-HPLC through a γ-ray flow detector.

In Vitro Stability, Pharmacokinetics, and Biodistribution of ^{18}F-PTTP

^{18}F-PTTP showed excellent stability in 0.9% NaCl and 0.1% bovine serum albumin at room temperature, with negligible falloff until about 6 h after labeling (Supplemental Fig. 1A; supplemental materials are available at http://jnm.snmjournals.org). The radioligand in mouse blood showed a fast clearance curve, with a very short half-life ($t_{1/2\alpha}$ = 2.13 ± 0.62 min, $t_{1/2\beta}$ = 31 ± 1.3 min) (Supplemental Fig. 1B). The biodistribution of the radiolabel to various organs at a series of time points is presented in Figure 2 as percentage injected dose per gram of tissue. Uptake of the radiolabel (^{18}F-PTTP) gradually decreased at subsequent time points in these organs, except for stomach and intestines. The uptake for stomach and intestines showed a slight increase for the first 15 min,

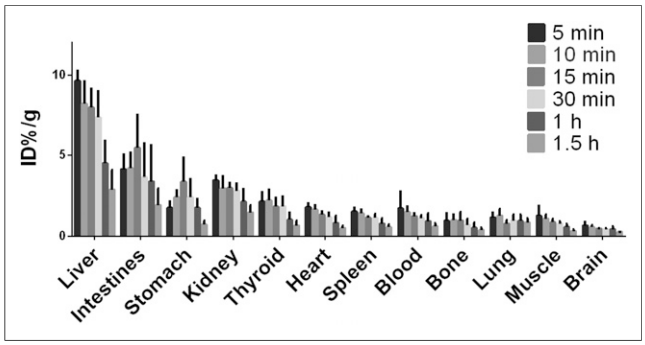

FIGURE 2. Biodistribution of ^{18}F-PTTP in BALB/c nude mice at 5, 10, 15, 30, 60, and 90 min after injection. %ID/g = percentage injected dose per gram of tissue.

followed by a decline at subsequent time points. We note that uptake in the liver and kidneys remained high, whereas uptake in the brain, lung, and muscle was consistently low in the time series.

Cell Line Receptor Expression Validation

Cell immunofluorescence staining revealed that the P2X7R (green) was localized mainly on the surface of RAW264.7 cells (Fig. 3B). The CD68 marker colocalizes on the same cell surfaces (red and yellow, Figs. 3A and 3C). A Western blot analysis compared expression of the P2X7R in the same mouse macrophage cell line to a series of human lung cancer cells lines (Fig. 3D). Analysis revealed that P2X7R expression was generally 3–4 times higher in RAW264.7 cells than in human lung cancer cell lines ($P < 0.05$). At the same time, Western blots showed P2X7R expression to be essentially identical (Fig. 3D) among the human cancer cell lines tested.

Radioligand Association and Saturation Kinetics Experiments

From the ligand binding assay (Supplemental Fig. 1C), we observed that the macrophage-bound fraction of radioligand increases with time, achieving a steady-state maximum in nearly 2 h. Dynamic binding rates of this magnitude support our protocol of using incubation periods of 2 h for achieving steady-state binding. In radioligand saturation binding assays, nonspecific binding of ^{18}F-PTTP remained relatively constant over the same cell density (2–5 × 10^5 RAW264.7 cells, Supplemental Fig. 1D). The specific binding curve, however, showed a typical sigmoidal shape, with binding affinity in the nanomolar range (K_d = 12.37 ± 2.204 nM, Supplemental Fig. 1D), indicating that ^{18}F-PTTP binds to the P2X7R with high affinity. Receptor density was 13.54 ± 0.3821 fmol/cell.

Small-Animal PET/CT Imaging

Figures 4A, 4B, and 4C show the PET/CT dynamic scans at 5 min after injection of representative animals in the inflammation, tumor, and blocked groups, respectively. The scans demonstrated localization of the radioaffinity label to the target in the inflammation cohort, indicating an apparent affinity between ^{18}F-PTTP and inflammatory muscle. Quantification of radiolabel uptake from scan images of target organs taken in a progressive time series (Table 1) show that uptake of the P2X7R ligand peaked at 5 min after injection (T/N = 2.17, n = 3). Moreover, within 15 min after injection, the T/N ratio of the inflammation group was always higher than the T/N ratio of the tumor tissue ($P < 0.05$), and there was still radiolabel uptake at 30 min after injection (T/N = 1.20, n = 3). The ^{18}F-PTTP probe had high physiologic uptake in fat, liver, and intestines, whereas brain, lung, and muscle showed lower physiologic uptake. However, no obvious uptake of the radiolabel in the A549 tumor was found at 5 min after injection (T/N = 1.01, n = 3) (Fig. 4B) or any other time point. Compared with the data obtained by^{18}F-FDG imaging (Table 1), the T/N ratio of ^{18}F-PTTP in inflammation-model mice was significantly higher than the uptake of the same marker in tumor-model mice (Table 1) ($P < 0.05$).

In blocking studies, we observed that the uptake of ^{18}F-PTTP in inflammatory muscles decreased significantly after 1 mg of cold PTTP had been injected 10 min before the radiolabel (Fig. 4C). The T/N ratio of the blocked group was significantly lower than that of the unblocked group as Table 1 shows ($P < 0.05$).

Histologic Analysis

The results of hematoxylin and eosin and immunofluorescence staining are shown in Figure 5. It is apparent that the inflammatory region identified by hematoxylin and eosin staining overlaps that identified by immunofluorescence staining. Immunofluorescence images show that P2X7R (green) and the CD68 receptor (red) are coexpressed in inflammatory tissues. Immunofluorescence staining for P2X7R (green) revealed weak fluorescence in tumor sites, whereas strong P2X7R fluorescence signal was observed in inflamed tissue (Fig. 5). Both tumor and inflamed muscle colocalized P2X7R (green) in macrophages (CD68, red) as visualized by the dual-labeled yellow cells (Fig. 4).

DISCUSSION

Most reported P2X7R radioligands have used short–half-life nuclides, such as ^{11}C (20.3 min), and the limited temporal window makes it difficult to allow adequate drug distribution for delivery to target in vivo. ^{18}F has a comparatively longer half-life (110 min), enabling it to be produced at a more distant cyclotron and then transported to other facilities. Thus, ^{18}F-labeled compounds have

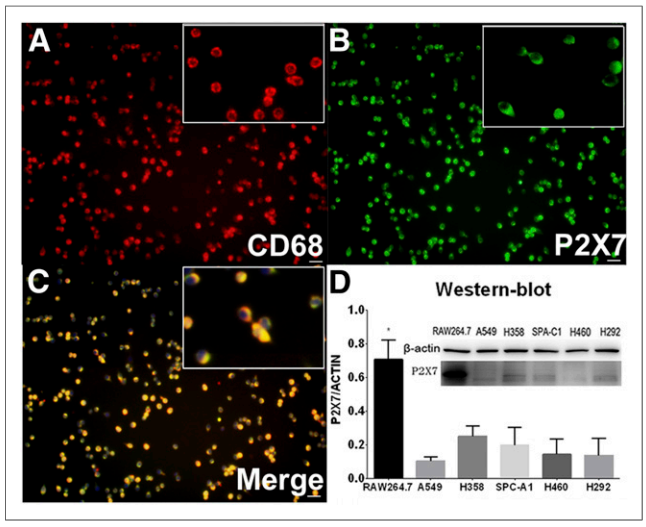

FIGURE 3. Validation of P2X7R expression in cultured RAW264.7 cell line. (A–C) Immunofluorescence staining of CD68 (A), P2X7 (B), and merged (C) images showing marker localization in RAW264.7 cell culture. Images show that P2X7R and CD68 are expressed mainly on RAW264.7 cell membranes. Scale bars = 20 μm. (D) Western blot of RAW264.7 and series of lung cancer lines.

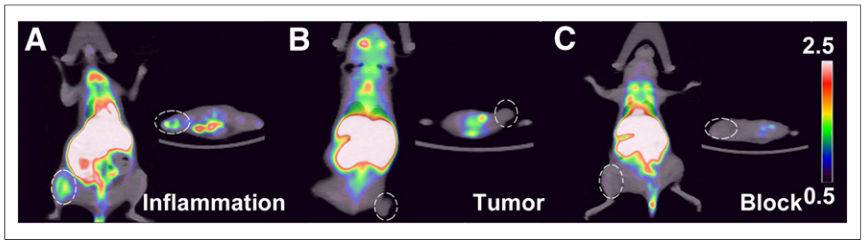

FIGURE 4. Small-animal PET/CT imaging and histologic analysis of ^{18}F-PTTP–injected mice: representative inflammation cohort (A), A549 tumor cohort (B), and competitively blocked cohort (C) at 5 min after injection. Elliptic dashed lines frame area of inflamed tissue (A), tumor graft (B), and blocked tissue (C).

greater potential for widespread clinical acceptance than ^{11}C-labeled compound (*20*). The usual way of attaching ^{18}F to an organic molecule is through an^{18}F-ethyl or ^{18}F-phenyl motif that conjugates to a reactive group on the target molecule. However, this usually requires 2-step or multiple-step radiosynthesis, compared with the quick, 1-step, ^{18}F-trifluoromethylation reaction used here. Furthermore, the ^{18}F-ethyl motif is often unstable under base or heated conditions, posing a high risk that a vinyl byproduct will form via an elimination reaction (*21*). For example, ^{18}F-IUR-1601 (*21*) and ^{18}F-EFB (*18*) are currently reported to be useful ^{18}F-labeled P2X7R radioligands; however, their short-term stability or complex synthetic pathways have limited their application. Compared with the fluoroethyl functionality, trifluoromethyl is a fairly stable functional group; it is therefore preferable to prepare the ^{18}F radiotracer by means of a ^{18}F-trifluoromethylation reaction.

PTTP, as a potent rat and human P2X7R antagonist, has good physicochemical properties, excellent P2X7R affinity (*22*), and rapid pharmacokinetic delivery. Moreover, by virtue of the trifluoromethyl addition, PTTP can be radiosynthesized without any modification of its chemical structure, leaving all its pharmaceutical effects preserved. To make allowance for the easy synthesis of precursor and convenient handling of reagents, we were motivated to try the direct addition of an ^{18}F-CF_3 group to an aryl iodine precursor as reported by Gouverneur and Passchier (*23*). ^{18}F-PTTP synthesis resulted in a good chemical purity and in vitro stability confirmed by reversed-phase HPLC. Its binding affinity was in the nanomolar range. In addition, simple and rapid chemistry and favorable pharmacokinetics make ^{18}F-PTTP useful for screening radioligand targeting against P2X7R receptors.

Unlike ^{11}C-A740003 (*14*), ^{18}F-PTTP could cross the blood–brain barrier in normal mice as shown in biodistribution studies (Fig. 2). Compared with the low brain uptake of ^{18}F-EFB in both healthy rats and rats treated with lipopolysaccharide before PET scanning (*18*), ^{18}F-PTTP shows additional potential for use in imaging microglial activation. In addition, its high uptake by liver and intestinal tissues suggests that elimination of ^{18}F-PTTP is mainly through hepatobiliary ducts, as is consistent with the lipophilicity of the tracer. The uptake by lung and muscle in normal mice is low, suggesting that the imaging agent might be useful as a tracer in pulmonary inflammation.

In our experiments, we chose a turpentine oil–induced inflammation model for PET imaging to evaluate the efficacy of ^{18}F-PTTP as a radiotracer for peripheral tissue inflammation. Focal entrapment of turpentine oil acted as a persistent stimulus that was difficult for macrophages (and other inflammatory cells) to eliminate. Acute inflammation in muscle will convert to chronic inflammation at 4–6 d after onset (*24,25*). Yamada et al. found that the optimal uptake of ^{18}F-FDG occurs at day 5 after inflammation onset (*24*). Consistent with this finding, we choose to use a protocol calling for a PET scan on day 5 after inflammation onset.

Figure 4A and Table 1 show that the peak uptake of ^{18}F-PTTP in inflamed muscles occurs at 5 min after injection. We speculate that the short residence period of the radiolabel may occur for 2 reasons: rapid blood clearance and reduced competitiveness for ligand at inflammatory sites that are under high concentrations of adenosine triphosphate. We presume that ^{18}F-PTTP and adenosine triphosphate share some of the same binding sites as P2X7R. Hematoxylin and eosin staining and immunofluorescence results confirmed that P2X7R is expressed mainly on macrophages that invade inflamed tissues, indirectly demonstrating that ^{18}F-PTTP can be used to visualize macrophage targets.

Although ^{18}F-FDG PET has been used for tumor detection, staging, and assessment of therapy and has provided useful

TABLE 1
Ratio of Target to Normal Muscle in Dynamic PET Images

		T/N			*P*	
Radioligand	Time (min)	Inflammation	Tumor	Block	Inflammation vs. tumor	Inflammation vs. block
^{18}F-PTTP	5	2.17 ± 0.37	1.01 ± 0.30	1.40 ± 0.21	0.009*	0.016*
	10	1.58 ± 0.17	0.88 ± 0.23	1.03 ± 0.01	0.020*	0.010*
	15	1.33 ± 0.15	0.98 ± 0.17	1.02 ± 0.01	0.021*	0.012*
	30	1.20 ± 0.14	0.96 ± 0.13	0.99 ± 0.02	0.093	0.048*
	45	1.04 ± 0.06	1.04 ± 0.15	—	0.966	—
	60	1.10 ± 0.11	1.03 ± 0.09	—	0.510	—
^{18}F-FDG	30	1.70 ± 0.40	1.72 ± 0.35	—	0.911	—

*$P < 0.05$.
Data are mean ± SD.

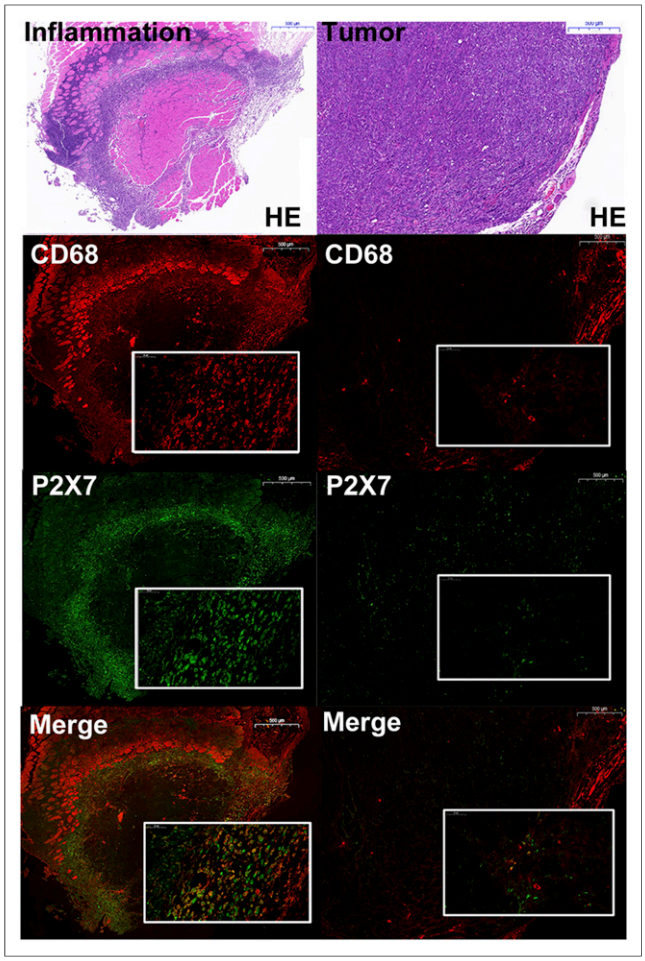

FIGURE 5. Histologic and immunofluorescence images of tissue sections from inflammation and tumor cohorts. HE = hematoxylin and eosin; scale bars = 500 μm; small rectangular frame = 50 μm.

information to evaluate infected lesions and inflammatory disorders, it has recognized limitations for differentiating tumors from nontumor inflammatory diseases (*4*). In recent years, researchers have recognized that expression of P2X7R in inflammatory cells may be associated with tumor cell carcinogenesis, proliferation, and metastasis (*26*). Our study set out to determine whether ^{18}F-PTTP PET/CT can be used to image tumors and differentiate them from inflamed tissues. On the basis of our biodistribution results, we selected human lung cancer cell lines as viable tumor models for ^{18}F-PTTP imaging. We screened the lung cancer cell lines by Western blot and found that the expression level of macrophage receptors was significantly higher in RAW264.7 cells than in any lung cancer cell line tested ($P < 0.05$).

Although we found a significant difference between uptake of ^{18}F-PTTP in tumor-model mice and in inflammation-model mice in a PET/CT dynamic scan at 5 min after injection (Table 1), the difference was insignificant after 1 h. This finding contrasts with the results for uptake of the ^{18}F-FDG probe, which was not significantly different between inflamed tissue and tumor even at 5 min after injection (Table 1, $P < 0.05$). Combined with the histologic analysis, we speculate that the low uptake in tumor is due to lower P2X7R expression and less macrophage invasion. Therefore, we conclude that ^{18}F-PTTP is a better probe to localize inflammatory diseases by screening for macrophages than to identify lung tumors. Further work is needed to support this conclusion.

CONCLUSION

In this article, we have described a novel ^{18}F-labeled P2X7R-targeted radioligand that was successfully used to track macrophage distributions in culture and in inflammation and tumor models in vivo. We described the reagent synthesis and our characterization, by various methods, of its binding affinity and biodistribution under animal model conditions. We provided supporting evidence that ^{18}F-PTTP offers great potential as a radiotracer and P2X7R antagonist for screening new drugs, quantifying expression of P2X7R in peripheral inflammation, and distinguishing inflammation from tumor.

DISCLOSURE

This study was funded by the National Nature Science Foundation of China (81471706, 11875114, 81871407), the Shanghai Science and Technology Committee International Collaboration Project (16410722700), the Shanghai Sailing Program (17YF1417400), and Open Large Infrastructure Research of the Chinese Academy of Sciences. No other potential conflict of interest relevant to this article was reported.

ACKNOWLEDGMENT

We acknowledge Ivey Choi for manuscript editing.

REFERENCES

1. Warnatsch A, Ioannou M, Wang Q, et al. Inflammation: neutrophil extracellular traps license macrophages for cytokine production in atherosclerosis. *Science.* 2015;349:316–320.
2. Glass CK, Saijo K, Winner B, et al. Mechanisms underlying inflammation in neurodegeneration. *Cell.* 2010;140:918–934.
3. Hotamisligil GS. Inflammation and metabolic disorders. *Nature.* 2006;444:860–867.
4. Vinay DS, Ryan EP, Pawelec G, et al. Immune evasion in cancer: mechanistic basis and therapeutic strategies. *Semin Cancer Biol.* 2015;35(suppl):S185–S198.
5. Coussens LM, Werb Z. Inflammation and cancer. *Nature.* 2002;420:860–867.
6. Tronel C, Largeau B, Santiago RM, et al. Molecular targets for PET imaging of activated microglia: the current situation and future expectations. *Int J Mol Sci.* 2017;18:802.
7. James ML, Belichenko NP, Shuhendler AJ, et al. ^{18}F-GE-180 PET detects reduced microglia activation after LM11A-31 therapy in a mouse model of Alzheimer's disease. *Theranostics.* 2017;7:1422–1436.
8. Owen DR, Yeo AJ, Gunn RN, et al. An 18-kDa translocator protein (TSPO) polymorphism explains differences in binding affinity of the PET radioligand PBR28. *J Cereb Blood Flow Metab.* 2012;32:1–5.
9. Bhattacharya A, Biber K. The microglial ATP-gated ion channel P2X7 as a CNS drug target. *Glia.* 2016;64:1772–1787.
10. Ory D, Celen S, Gijsbers R, et al. Preclinical evaluation of a P2X7 receptor-selective radiotracer: PET studies in a rat model with local overexpression of the human P2X7 receptor and in nonhuman primates. *J Nucl Med.* 2016;57:1436–1441.
11. Bartlett R, Stokes L, Sluyter R. The P2X7 receptor channel: recent developments and the use of P2X7 antagonists in models of disease. *Pharmacol Rev.* 2014;66:638–675.
12. Adinolfi E, Capece M, Franceschini A, et al. Accelerated tumor progression in mice lacking the ATP receptor P2X7. *Cancer Res.* 2015;75:635–644.
13. De Marchi E, Orioli E, Dal Ben D, et al. P2X7 receptor as a therapeutic target. *Adv Protein Chem Struct Biol.* 2016;104:39–79.

14. Janssen B, Vugts DJ, Funke U, et al. Synthesis and initial preclinical evaluation of the P2X7 receptor antagonist ^{11}C-A-740003 as a novel tracer of neuroinflammation. *J Labelled Comp Radiopharm.* 2014;57:509–516.
15. Fantoni ER, Dal BD, Falzoni S, et al. Design, synthesis and evaluation in an LPS rodent model of neuroinflammation of a novel ^{18}F-labelled PET tracer targeting P2X7. *EJNMMI Res.* 2017;7:31.
16. Beaino W, Janssen B, Kooij G, et al. Purinergic receptors P2Y12R and P2X7R: potential targets for PET imaging of microglia phenotypes in multiple sclerosis. *J Neuroinflammation.* 2017;14:259.
17. Territo PR, Meyer JA, Peters JS, et al. Characterization of ^{11}C-GSK1482160 for targeting the P2X7 receptor as a biomarker for neuroinflammation. *J Nucl Med.* 2017;58:458–465.
18. Ory D, Celen S, Gijsbers R, et al. Preclinical evaluation of a P2X7 receptor-selective radiotracer: PET studies in a rat model with local overexpression of the human P2X7 receptor and in nonhuman primates. *J Nucl Med.* 2016;57:1436–1441.
19. Janssen B, Vugts DJ, Wilkinson SM, et al. Identification of the allosteric P2X7 receptor antagonist ^{11}C-SMW139 as a PET tracer of microglial activation. *Sci Rep.* 2018;8:6580.
20. Dickstein LP, Zoghbi SS, Fujimura Y, et al. Comparison of ^{18}F- and ^{11}C-labeled aryloxyanilide analogs to measure translocator protein in human brain using positron emission tomography. *Eur J Nucl Med Mol Imaging.* 2011;38:352–357.
21. Gao M, Wang M, Glick-Wilson BE, et al. Synthesis and preliminary biological evaluation of a novel P2X7R radioligand ^{18}F-IUR-1601. *Bioorg Med Chem Lett.* 2018;28:1603–1609.
22. Savall BM, Wu D, De AM, et al. Synthesis, SAR, and pharmacological characterization of brain penetrant P2X7 receptor antagonists. *ACS Med Chem Lett.* 2015;6:671–676.
23. Huiban M, Tredwell M, Mizuta S, et al. A broadly applicable ^{18}F-trifluoromethylation of aryl and heteroaryl iodides for PET imaging. *Nat Chem.* 2013;5:941–944.
24. Yamada S, Kubota K, Kubota R, et al. High accumulation of fluorine-18-fluorodeoxyglucose in turpentine-induced inflammatory tissue. *J Nucl Med.* 1995;36:1301–1306.
25. Reubi JC, Waser B, Maecke H, et al. Highly increased ^{125}I-JR11 antagonist binding in vitro reveals novel indications for SST2 targeting in human cancers. *J Nucl Med.* 2017;58:300–306.
26. Hofman P, Cherfilsvicini J, Bazin M, et al. Genetic and pharmacological inactivation of the purinergic P2X7 receptor dampens inflammation but increases tumor incidence in a mouse model of colitis-associated cancer. *Cancer Res.* 2015;75:835–845.